Computation of EFIE Matrix Entries With Singular Basis Functions

Roberto D. Graglia, *Fellow, IEEE*, Andrew F. Peterson, *Fellow, IEEE*, and Paolo Petrini

***Abstract*— The use of singular basis functions enhances the convergence of method-of-moments (MoM) solutions for structures containing edges. While standard algorithms for computing the MoM matrix entries treat Green's function singularities, these are not well-suited for integrating the singular basis functions: conventional quadrature routines exhibit slow convergence and may produce inaccurate results. In this paper, new algorithms are proposed for handling the combination of edge singularities and Green's function singularities on quadrilateral cells.**

***Index Terms*— Basis functions, hierarchical basis functions, method of moments (MoM), singular basis functions, wedges.**

I. Introduction

THE basic electric-field integral equation (EFIE) matrix entries for interactions between two curved patches have the form [1]

$$Z_{mn} = j\omega\mu \iint_{\text{obs}} \iint_{\text{src}} \boldsymbol{T}_m(\boldsymbol{r}) \cdot \boldsymbol{B}_n(\boldsymbol{r}')\, G\, d\boldsymbol{r}'\, d\boldsymbol{r} + \frac{1}{j\omega\epsilon} \times \iint_{\text{obs}} \nabla \cdot \boldsymbol{T}_m(\boldsymbol{r}) \iint_{\text{src}} \nabla' \cdot \boldsymbol{B}_n(\boldsymbol{r}')\, G\, d\boldsymbol{r}'\, d\boldsymbol{r} \quad (1)$$

where

$$G = \frac{\exp(-jkR)}{4\pi R} \quad (2)$$

is the free space Green's function and

$$R = |\boldsymbol{r} - \boldsymbol{r}'| \quad (3)$$

is the distance between the observation ($\boldsymbol{r}$) and the source ($\boldsymbol{r}'$) point. Index m is used to denote a specific vector testing function ($\boldsymbol{T}_m$) on the observer patch (or patches) while index n is used to denote a specific vector basis function ($\boldsymbol{B}_n$) on the source patch (or patches). In practice, patches are mapped from the curved child domain to a reference or parent domain for evaluation, and in fact testing and basis functions are conveniently defined in the parent domain [1]. For example, a curved quadrilateral cell of the child domain, described in coordinates (x, y, z), is mapped by the planar *parent* square patch $\{0 \le \xi_1 \le 1; 0 \le \xi_2 \le 1\}$ of a parent (ξ_1, ξ_2)-frame.

Manuscript received May 4, 2018; revised July 17, 2018; accepted August 12, 2018. Date of publication September 6, 2018; date of current version October 29, 2018. *(Corresponding author: Roberto D. Graglia.)*

R. D. Graglia and P. Petrini are with the Dipartimento di Elettronica e Telecomunicazioni, Politecnico di Torino, 10129 Turin, Italy (e-mail: roberto.graglia@polito.it; paolo.petrini@polito.it).

A. F. Peterson is with the School of Electrical and Computer Engineering, Georgia Institute of Technology, Atlanta, GA 30332 USA (e-mail: peterson@ece.gatech.edu).

Color versions of one or more of the figures in this paper are available online at http://ieeexplore.ieee.org.

Digital Object Identifier 10.1109/TAP.2018.2868979

In the following, for the quadrilateral patch, we also use the dependent parent coordinates:

$$\xi_3 = 1 - \xi_1 \quad (4)$$

$$\xi_4 = 1 - \xi_2 \quad (5)$$

to number the cell edges from one to four, with the mth edge lying along the coordinate line $\xi_m = 0$. The Jacobian $\mathcal{J}_\xi(\boldsymbol{\xi})$ of the transformation from parent-to-child coordinates is a polynomial of the parent variables whose order grows with the growth of the order of the transformation (that is, with the degree of curvature of the child cell), while the coefficients of $\mathcal{J}_\xi$ depend on the position in the child space of the *driving* points used to define the transformation [1].

A single matrix entry (Z_{mn}) may require integrals over as many as four cells, since each vector basis or testing function may straddle two cells. For brevity, the following discussion considers a single (curved) quadrilateral source cell mapped to a parent square cell with domain $\{0 \le \xi_1 \le 1; 0 \le \xi_2 \le 1\}$ and an observer fixed at some location $\boldsymbol{r}$ in the child space that corresponds to a local observer parent coordinate (u, v). In general, the u and v coordinates of the observation point are obtained by solving a nonlinear system, which is not a straightforward problem apart from the very simple case of bilinear mapping. We also specialize to the following.

1) Source and observer cells that lie in the same child plane.
2) A basis function that exhibits an edge singularity with the behavior $\xi_1^{\nu-1}$ at edge 1 ($\xi_1 = 0$) of that domain.
3) ν in the range $1/2 \le \nu < 1$. Extension of the results to deal with polynomial bases is obtained by setting $\nu = 1$.

Although matrix entries for triangular and quadrilateral cells involving *polynomial* vector testing ($\boldsymbol{T}_m$) and basis ($\boldsymbol{B}_n$) functions are extensively discussed elsewhere (see [1]–[17] and references therein), the novelty of this paper consists precisely in being able to treat vector functions that are unbounded along one side of the cell.

While the following is restricted to quadrilateral cells, the technique shown here can be easily adapted to triangles. (In the following, for example, whenever we subdivide the quadrilateral cell into subtriangles to cancel Green's function singularity we remap the basis functions $\boldsymbol{B}_n$ in terms of pseudopolar coordinates. The extension to triangular cells simply requires the use of a different, appropriate remapping.)

In this connection, we also observe that it may be more convenient to model edge singularities using quadrilateral elements instead of triangular ones, because the latter require the introduction of triangles with only one vertex attached to the singular edge [18, Sec. III-D], [19]. As discussed

in [18, Sec. III-D], bases on such cells require additional information to align them with the edge and may reduce accuracy if not properly aligned. Preliminary results of this paper were presented in [20].

We consider three cases of interest, based on the relative location of the observer with the source cell (see Fig. 1).

II. Observer Not in the Source Cell and Not Very Close to the Source Cell

After mapping to the parent domain, the inner integrals over the source patch in (1) have the form

$$I = \int_0^1 \int_0^1 \xi_1^{\nu-1}\, f(\xi_1,\xi_2)\, G(\xi_1,\xi_2)\, \mathcal{J}_\xi(\xi_1,\xi_2)\, d\xi_1\, d\xi_2 \quad (6)$$

where G is a Green's function such as (2), $\mathcal{J}_\xi$ is the Jacobian of the transformation from parent to child domain, and the function f contains the rest of the basis function. The edge singularity at $\xi_1 = 0$ can be canceled by a second transformation in terms of the variable

$$\zeta_1 = \xi_1^\nu. \quad (7)$$

We observe that

$$\xi_1 = \zeta_1^{1/\nu} \quad (8)$$

$$d\xi_1 = \frac{1}{\nu}\zeta_1^{(1/\nu-1)} d\zeta_1 = \frac{1}{\nu}\xi_1^{1-\nu} d\zeta_1. \quad (9)$$

Thus, the Jacobian of this transformation cancels the factor $\xi_1^{\nu-1}$ in (6). Furthermore, the limits of integration transform as

$$\xi_1 = 0 \Rightarrow \zeta_1 = 0 \quad (10)$$

$$\xi_1 = 1 \Rightarrow \zeta_1 = 1. \quad (11)$$

Therefore, we obtain

$$I = \frac{1}{\nu}\int_0^1 \int_0^1 f\left(\zeta_1^{1/\nu},\xi_2\right)\, G\left(\zeta_1^{1/\nu},\xi_2\right)\, \mathcal{J}_\xi\left(\zeta_1^{1/\nu},\xi_2\right)\, d\zeta_1\, d\xi_2. \quad (12)$$

In the event that the observer (u, v) is sufficiently far from the source cell so that Green's function singularity is not an issue, the integration in (12) can be performed by quadrature over the square reference cell without further transformation. Although the basis functions are defined in the $\boldsymbol{\xi}$-parent space, the integral (12) is actually performed in a *grandparent* space $\{\zeta_1 = \xi_1^\nu, \zeta_2 = \xi_2\}$.

III. Self- and Near-Self-Source Integrals

Conversely, in the self- and near-self-regions (see Fig. 1), we cancel the singularities of the integrands by using a pair of integral transformations in an order that depends on the sign of the parent observer coordinate u. For $u \geq 0$, we first cancel the singularity of $\xi_1^{\nu-1}$ (as discussed in Section II) whereas, for $u < 0$, we first cancel the singularity of Green's function. The sequence of the transformations for positive u-values must be different than that used for negative u-values to eliminate the singularities in the integration interval; the singularities would not be canceled if the order of the transformations

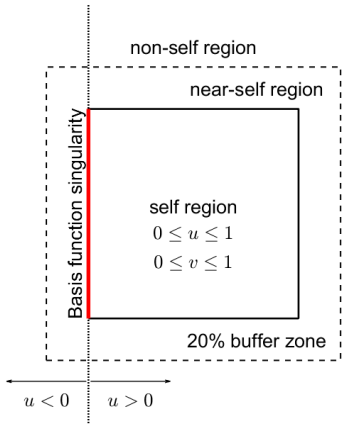

Fig. 1. Depiction of different regions around the source cell. The nearly singular cases occur when the observer is close to the source cell, typically in a 20% buffer range from $-0.2 < u < 0$, $1.0 < u < 1.2$, $-0.2 < v < 0$, $1.0 < v < 1.2$. Because of the transformation in (7), the case $u < 0$ must be treated differently from $u > 0$.

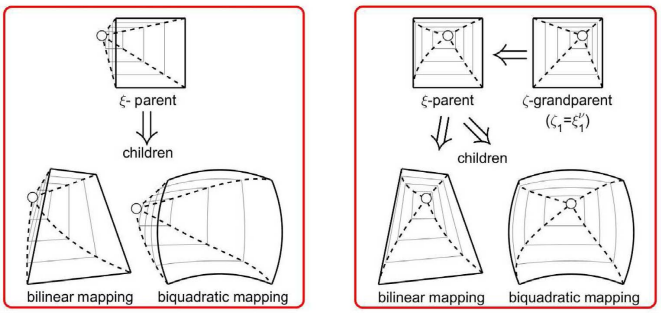

Fig. 2. Two-quadrilateral children (at bottom), and their parent and grandparent square cells (at top) are shown with solid lines. A circle marks the observation point. Left: four *rectilinear* triangles of the parent space used to deal with observation points located in the $\xi_1 < 0$ half-space; in this case, one integrates in the parent space. Right: four *rectilinear* triangles of the grandparent space used to deal with observation points located in the $\xi_1 \geq 0$ half-space; in this case, one integrates in the grandparent space.

was inverted. Likewise, by inverting the order of the transformations for $u < 0$, the integration variables and limits become complex valued.

What happens in the various spaces (child, parent, and grandparent) with the two different transformation sequences is graphically represented in Fig. 2, where a circle marks the observation point [$\boldsymbol{r}$ in the child, (u, v) in the parent, and (u^ν, v) in the grandparent space]. In Fig. 2, the *parent* square-patch maps two different quadrilateral children: the bottom-left child is obtained with bilinear mapping using four interpolatory points, while the child at bottom-right is obtained by biquadratic mapping using nine interpolatory points. Fig. 2 considers the case of $\nu = 1/2$; the $u < 0$ case (precisely the case of $u = -0.2, v = 0.75$) is shown at left, whereas the right-hand side of Fig. 2 shows the case for $u > 0$ (namely, $u = 0.5$ and $v = 0.75$).

A. Polar Variables, Polar Transformation, and Green's Singularity Cancellation

To cancel the Green's function singularity, we use a polar transform (other schemes such as Duffy [21], [22], arcsinh, and tanh-sinh may be used as alternatives and can be substituted

TABLE I
POLAR TO PARENT/GRANDPARENT VARIABLES MAPPING

For $u < 0$				
	T_1	T_3	T_2	T_4
h_i	u	$1-u$	v	$1-v$
ξ_1	$\lambda\, u$	$1-\lambda(1-u)$	$\sigma+\lambda(u-\sigma)$	$1-\sigma+\lambda[u-(1-\sigma)]$
ξ_2	$\lambda[v-(1-\sigma)]+(1-\sigma)$	$\lambda(v-\sigma)+\sigma$	λv	$1-\lambda(1-v)$
For $u \geq 0$				
	T_1	T_3	T_2	T_4
h_i	u^ν	$1-u^\nu$	v	$1-v$
ζ_1	$\lambda\, u^\nu$	$1-\lambda(1-u^\nu)$	$\sigma+\lambda(u^\nu-\sigma)$	$1-\sigma+\lambda[u^\nu-(1-\sigma)]$
ζ_2	$\lambda[v-(1-\sigma)]+(1-\sigma)$	$\lambda(v-\sigma)+\sigma$	λv	$1-\lambda(1-v)$

The source-integration package integrates in the polar-frame (λ, σ) and has on input (apart other parameters) the u, v, and ν values. The parent/gandparent coordinates of the integration point are functions of λ, σ, evaluated as in the Table. Notice that for $u \geq 0$ one has $\xi_1 = \zeta_1^{1/\nu}$, $\xi_2 = \zeta_2$. The basis function factor $f(\boldsymbol{\xi})$ is a function of the parent-variables computed in terms of the integration-point parent coordinates ξ_1, ξ_2, $\xi_3 = 1-\xi_1$, and $\xi_4 = 1-\xi_2$. Once the $\boldsymbol{\xi}$-coordinates are known, the position of the integration point $\boldsymbol{r}'$ in the child-space, and the distance R from integration to observation point are computed by use of the parent-to-child mapping. Finally, the integration package evaluates the ratio $(1-\lambda)/R$ and the value of the integrand together with the relevant weight at the integration point.

for the following with minor differences in the change-of-variables; the double-exponential scheme [11] may also be useful for near-singular interactions for the singular-basis functions). The polar transform is used for illustration and, while it has worked well in our tests, we have not compared its performance with the other near field cancellation scheme and make no claim as to its optimality. We believe that the proposed algorithm can be adapted to any cancellation scheme, so that one can introduce singular vector basis functions and numerically evaluate all the required integrals with acceptable accuracy. In addition, in our method-of-moments (MoM) applications using singular basis functions [23], we often use adaptive quadrature that may help compensate for a "poor" near-singular algorithm.

With reference to Fig. 2, the observation point defines four-*curved* subtriangles (dashed lines) of the child space, numbered with the number that labels the edge on which they are based. These triangles are mapped by rectilinear triangles of the parent space for $u < 0$ and by rectilinear triangles of the grandparent space for $u > 0$. Within each rectilinear triangle, we introduce new variables (λ, σ) with σ increasing from 0 to 1 in the counterclockwise sense around the vertex. The segment $\{\lambda = 0;\ 0 \leq \sigma \leq 1\}$ maps the ith edge of the cell, and $\lambda = 1$ is the point that maps onto $\boldsymbol{r}$, eventually. Fig. 2 reports in gray the λ =0.25, 0.5, and 0.75 coordinate lines.

The Jacobian of the transformation from pseudopolar (λ, σ) to grandparent (if $u \geq 0$) or parent ($u < 0$) coordinates is

$$\mathcal{J}_i = h_i(1-\lambda) \tag{13}$$

where h_i is the height of the ith rectilinear subtriangle measured with respect to the ith edge (h_i can be negative). Table I reports, for each subtriangle T_i (for $i = 1, 4$), the expressions of the parent/grandparent variables in terms of the polar variables and the value of the height h_i. $\mathcal{J}_i$ has a first order zero at $\lambda = 1$ that cancels the singularity of Green's function occurring when observation and integration points coincide. In fact, in the *child* space, the distance from $\boldsymbol{r}$ to an integration point of the ith subtriangle vanishes at $\lambda = 1$ in accordance with

$$R = |\boldsymbol{r} - \boldsymbol{r}'| = (1-\lambda)\, d_i. \tag{14}$$

The ratio

$$\frac{(1-\lambda)}{R} = \frac{1}{d_i} \tag{15}$$

remains finite as $\lambda \to 1$, $R \to 0$ and is numerically computed on-the-fly for all λ by using the parent-to-child mapping shown at the bottom of Fig. 2. This removes Green's function singularity and permits the evaluation of the integrals by quadrature. In this connection, we also observe that, normally, open integration routines are used that do not sample the integrand at the integration border, that is, at $\lambda = 1$. (For λ-values close to unity and for children-cells that are not excessively distorted, the dependence on σ of the function d_i does not vary too much with λ and can, therefore, be easily extrapolated to obtain the value of d_i at $\lambda = 1$, if this is really needed.)

To reduce the integration burden, it is very convenient to integrate only on the subregion of the triangular domain that belongs to the parent/grandparent square patch (see Fig. 3). This is easily accomplished by reducing the upper limit of the λ-integral to a value λ_E smaller than unity. Table II summarizes the algorithm to evaluate λ_E when dealing with basis factors of the form $\xi_1^{\nu-1} f(\boldsymbol{\xi})$. Clearly, in this manner, one does not need to compute the integral contribution of the triangle T_i whenever its height h_i (as reported in Table I) is negative. However, this requires one to integrate first on λ (inner source integral) and then on σ (outer source integral) by using 1-D integration routines. (As said, ad hoc integration algorithms to directly compute the double integral on the triangular simplexes could be used whenever $0 \leq u \leq 1$, $0 \leq v \leq 1$.)

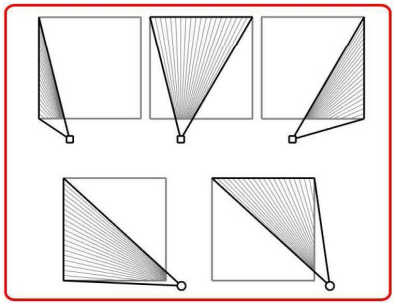

Fig. 3. We integrate only on the subregion of the triangular domains that belongs to the square parent/grandparent patch. In this manner, for observation point (u, v) located on the border or outside the patch, only three (top figure) or two (bottom figure) subtriangles are involved. These subregions get triangular or trapezoidal shape and are defined by an appropriate value of λ_E. Table II summarizes the algorithm that defines these subregions. At top, the *grandparent* observation point is located at $(u^\nu, v) = (0.3, -0.2)$ (square marker); at bottom (circular marker), it is placed at $(u^\nu, v) = (1.15, -0.05)$.

TABLE II

λ_E FUNCTION

	$\lambda_E = \min(\lambda_U, \lambda_V)$			
	λ_U (default value $= 1$)		λ_V (default value $= 1$)	
	If $u \le 0$	If $u \ge 1$	If $v \le 0$	If $v \ge 1$
T_1	0 (not exp.)	$\dfrac{1}{u^\nu}$	$\dfrac{1-\sigma}{1-\sigma-v}$	$\dfrac{\sigma}{\sigma+v-1}$
T_3	$\dfrac{1}{1-u}$	0 (not exp.)	$\dfrac{\sigma}{\sigma-v}$	$\dfrac{1-\sigma}{v-\sigma}$
T_2	$\dfrac{\sigma}{\sigma-u}$	$\dfrac{1-\sigma}{u^\nu-\sigma}$	0 (not exp.)	$\dfrac{1}{v}$
T_4	$\dfrac{1-\sigma}{1-\sigma-u}$	$\dfrac{\sigma}{u^\nu-(1-\sigma)}$	$\dfrac{1}{1-v}$	0 (not exp.)

The Table summarizes the algorithm to evaluate the λ_E function under the assumption that the source inner-integral is on λ while the outer one is on σ; that is, λ_E is a function of σ and of the (u, v) coordinates of the observer. For given σ, v and u values, we compute λ_V and λ_U and then obtain $\lambda_E = \min(\lambda_U, \lambda_V)$. The Table does take into account the fact that for $u \ge 0$ we integrate on sub-triangles of the grandparent space (this is why u is elevated to the ν power for $u > 0$) while, for $u < 0$, we integrate on sub-triangles of the parent space.

IV. Integral Recipes

A. Self-Cell and Nearly Singular: Case of $u \ge 0$

The results of Section III readily apply to the $u \ge 0$ case to integrate numerically on the grandparent cell. The sequence of the mappings to be used in this case is summarized in Fig. 4. On each subtriangle T_i, the integrals in polar coordinates (λ, σ) are used to compute, in sequence, the $\boldsymbol{\zeta}$, $\boldsymbol{\xi}$, and child coordinates of the integration point; the final expressions of these integrals are

$$\iint_{T_1} G\, f(\boldsymbol{\xi})\, \xi_1^{\nu-1} \mathrm{d}T_1 = \frac{u^\nu}{4\pi\, \nu} \int_0^1 \int_0^{\lambda_E} e^{-jkR}\, f(\boldsymbol{\xi}) \left(\frac{1-\lambda}{R}\right) \mathcal{J}_\xi \,\mathrm{d}\lambda \mathrm{d}\sigma \tag{16}$$

$$\iint_{T_3} G\, f(\boldsymbol{\xi})\, \xi_1^{\nu-1} \mathrm{d}T_3 = \frac{1-u^\nu}{4\pi\, \nu} \int_0^1 \int_0^{\lambda_E} e^{-jkR}\, f(\boldsymbol{\xi}) \left(\frac{1-\lambda}{R}\right) \mathcal{J}_\xi \,\mathrm{d}\lambda \mathrm{d}\sigma \tag{17}$$

$$\begin{array}{l} \dfrac{1}{4\pi\,\nu} \displaystyle\sum_{i=1}^{4} \int_{T_i} e^{-jkR}\, f(\boldsymbol{\xi})\, \left(\tfrac{1-\lambda}{R}\right)\, h_i\, \mathcal{J}_\xi \,\mathrm{d}\lambda \mathrm{d}\sigma \\ \qquad \Downarrow \qquad\qquad \Uparrow \mathrm{d}\zeta_1 \mathrm{d}\zeta_2 = h_i(1-\lambda) \\ \dfrac{1}{4\pi\,\nu} \displaystyle\sum_{i=1}^{4} \int_{T_i} e^{-jkR}\, f(\boldsymbol{\xi})\, \tfrac{1}{R}\, \mathcal{J}_\xi \,\mathrm{d}\zeta_1 \mathrm{d}\zeta_2 \\ \qquad \Downarrow \qquad\qquad \Uparrow \nu \xi_1^{\nu-1} \mathrm{d}\xi_1\, \mathrm{d}\xi_2 = \mathrm{d}\zeta_1 \mathrm{d}\zeta_2 \\ \dfrac{1}{4\pi} \displaystyle\int_{\boldsymbol{\xi}} e^{-jkR}\, f(\boldsymbol{\xi})\, \tfrac{\xi_1^{\nu-1}}{R}\, \mathcal{J}_\xi \,\mathrm{d}\xi_1\, \mathrm{d}\xi_2 \\ \qquad \Downarrow \qquad\qquad \Uparrow \mathrm{d}x\, \mathrm{d}y = \mathcal{J}_\xi \mathrm{d}\xi_1\, \mathrm{d}\xi_2 \\ \dfrac{1}{4\pi} \displaystyle\int_{\text{child}} e^{-jkR}\, f(\boldsymbol{\xi})\, \tfrac{\xi_1^{\nu-1}}{R}\, \mathrm{d}x\, \mathrm{d}y \end{array}$$

Fig. 4. Flow diagram assumes a singular basis function of the form $\xi_1^{\nu-1} f(\boldsymbol{\xi})$ and should be read bottom up. At bottom, the source integral on the quadrilateral child is up-transformed into an integral on the parent square cell of the $\boldsymbol{\xi}$-space, that is, the space where the basis functions are conveniently defined. The singular factor $\xi_1^{\nu-1}$ is canceled by setting $\zeta_1 = \xi_1^\nu$ (and $\zeta_2 = \xi_2$). Four *rectilinear* subtriangles are obtained by joining the observation point to the four corner nodes of the ζ-parent cell (see Fig. 2). Finally, each subintegral on the four subtriangles is performed into a pseudopolar space (λ, σ) to cancel Green's function singularity.

$$\iint_{T_2} G\, f(\boldsymbol{\xi})\, \xi_1^{\nu-1} \mathrm{d}T_2 = \frac{v}{4\pi\, \nu} \int_0^1 \int_0^{\lambda_E} e^{-jkR}\, f(\boldsymbol{\xi}) \left(\frac{1-\lambda}{R}\right) \mathcal{J}_\xi \,\mathrm{d}\lambda \mathrm{d}\sigma \tag{18}$$

$$\iint_{T_4} G\, f(\boldsymbol{\xi})\, \xi_1^{\nu-1} \mathrm{d}T_4 = \frac{1-v}{4\pi\, \nu} \int_0^1 \int_0^{\lambda_E} e^{-jkR}\, f(\boldsymbol{\xi}) \left(\frac{1-\lambda}{R}\right) \mathcal{J}_\xi \,\mathrm{d}\lambda \mathrm{d}\sigma \tag{19}$$

where the value of λ_E depends on the subtriangle considered, as given in Table II, and can be equal to zero for some σ values. As said, the integral on T_3 is not computed for $u \ge 1$; similarly, the integral on T_2 and T_4 are not computed for $v \le 0$ and $v \ge 1$, respectively. In such occurrences, the computer code must assign to these subintegrals a default zero value.

Integration routines that are adaptive or of an appropriate (high) order should be used to evaluate the previous integrals, since the polar transformation distorts the basis functions and/or increases the order of the function $f(\boldsymbol{\xi})$. [To clarify this, just notice from Table I that the factor $v\, f(\boldsymbol{\xi})(1-\lambda)$ in (18), and $(v-1)\, f(\boldsymbol{\xi})(1-\lambda)$ in (19) simplify into $(v-\xi_2) f(\boldsymbol{\xi})$ if $u = 0$; these factors vanish at $\lambda = 1$, $\xi_2 = v$.]

B. Nearly Singular: Case of $u < 0$

Conversely, for $u < 0$, we integrate numerically on the parent cell and always set to zero the value of the subintegral on the first triangle T_1. The singular $\xi_1^{\nu-1}$ factor is canceled from the integrand by using, on each of the remaining three triangles T_i (for $i = 2, 3, 4$), a new transformation from the ζ to λ coordinate

$$\xi_1 = \zeta^{1/\nu} = \lambda\, \alpha_i + \beta_i \tag{20}$$

$$\lambda = \frac{1}{\alpha_i}(\zeta^{1/\nu} - \beta_i) \tag{21}$$

$$\xi_1^{\nu-1} \mathrm{d}\lambda = \frac{1}{\nu\, \alpha_i} \mathrm{d}\zeta \tag{22}$$

TABLE III

φ TO σ AND (ζ, φ) TO λ MAPPINGS USED FOR $u < 0$

	$\xi_1 = \zeta^{1/\nu} = \lambda\,\alpha_i + \beta_i$			
	α_i	β_i	λ	σ
T_3	$u-1$	1	$\dfrac{\zeta^{1/\nu}-1}{u-1}$	φ
T_2	$u-\sigma$	σ	$\dfrac{\zeta^{1/\nu}-\sigma}{u-\sigma}$	$u+\dfrac{1}{\varphi}$
T_4	$u-(1-\sigma)$	$1-\sigma$	$\dfrac{\zeta^{1/\nu}-(1-\sigma)}{u-(1-\sigma)}$	$1-\left(u+\dfrac{1}{\varphi}\right)$

TABLE IV

EXPRESSIONS OF THE $\boldsymbol{\xi}$-PARENT VARIABLES USED FOR $u < 0$

	ξ_1	ξ_2	
T_3	$\zeta^{1/\nu}$	$\dfrac{(1-\xi_1)v+(\xi_1-u)\sigma}{1-u}$	
T_2	$\zeta^{1/\nu}$	$\dfrac{(\sigma-\xi_1)v}{\sigma-u}$	$v-v\,(\xi_1-u)\,\varphi$
T_4	$\zeta^{1/\nu}$	$\dfrac{(1-\sigma-\xi_1)v+(\xi_1-u)}{1-\sigma-u}$	$v+(1-v)\,(\xi_1-u)\,\varphi$

ξ_1 depends only on the ζ integration variable of the inner integral while φ (or σ) are fixed by the outer integral, to yield the unique value of ξ_2 reported in the Table as function of φ (or σ). Recall that $\xi_3 = 1-\xi_1$, and $\xi_4 = 1-\xi_2$. The reported expressions are obtained from Table I and III.

to obtain

$$\iint_{T_3} G\,f(\boldsymbol{\xi})\,\xi_1^{\nu-1}\mathrm{d}T_3 = \frac{1}{4\pi\,\nu}\int_0^1 \frac{1}{1-u}\left\{\int_{\min_3}^1 e^{-jkR}\left(\frac{\xi_1-u}{R}\right)\mathcal{J}_\xi(\boldsymbol{\xi})\,f(\boldsymbol{\xi})\,\mathrm{d}\zeta\right\}\mathrm{d}\sigma \tag{23}$$

$$\iint_{T_2} G\,f(\boldsymbol{\xi})\,\xi_1^{\nu-1}\mathrm{d}T_2 = \frac{v}{4\pi\,\nu}\int_0^1 \frac{1}{(\sigma-u)^2}\left\{\int_{\min_2}^{\sigma^\nu} e^{-jkR}\left(\frac{\xi_1-u}{R}\right)\mathcal{J}_\xi(\boldsymbol{\xi})\,f(\boldsymbol{\xi})\,\mathrm{d}\zeta\right\}\mathrm{d}\sigma \tag{24}$$

$$\iint_{T_4} G\,f(\boldsymbol{\xi})\,\xi_1^{\nu-1}\mathrm{d}T_4 = \frac{1-v}{4\pi\,\nu}\int_0^1 \frac{1}{(1-\sigma-u)^2} \times\left\{\int_{\min_4}^{(1-\sigma)^\nu} e^{-jkR}\left(\frac{\xi_1-u}{R}\right)\mathcal{J}_\xi(\boldsymbol{\xi})\,f(\boldsymbol{\xi})\,\mathrm{d}\zeta\right\}\mathrm{d}\sigma \tag{25}$$

with α_i, β_i as in Table III, λ_E as in Table II, and

$$\min_3 = [1-\lambda_E(1-u)]^\nu \tag{26}$$

$$\min_2 = [\sigma+\lambda_E(u-\sigma)]^\nu \tag{27}$$

$$\min_4 = \{1-\sigma+\lambda_E[u-(1-\sigma)]\}^\nu. \tag{28}$$

Once again, observe that the ratio $(\xi_1-u)/R$ remains finite as $\xi_1 \to u$, $R \to 0$.

It should be clear why this sequence of transformations cannot be used to deal with $u \geq 0$ because of the presence of a pole in σ for the T_2 and T_4 integrands. The pole is at $\sigma = u$ and at $\sigma = 1-u$ for the T_2 and T_4 integrand, respectively. In case the pole gives numerical problems, that is for $|u|$ very close to zero, one should resort to another transformation from σ to φ coordinate to get [see Table III for the expressions of $\sigma(\varphi)$ and recall that $u < 0$]

$$\iint_{T_2} G\,f(\boldsymbol{\xi})\,\xi_1^{\nu-1}\mathrm{d}T_2 = \frac{v}{4\pi\,\nu}\int_{\frac{1}{1-u}}^{\frac{1}{-u}} = \left\{\int_{\min}^{\max} e^{-jkR}\left(\frac{\xi_1-u}{R}\right)\mathcal{J}_\xi(\boldsymbol{\xi})\,f(\boldsymbol{\xi})\,\mathrm{d}\zeta\right\}\mathrm{d}\varphi \tag{29}$$

$$\iint_{T_4} G\,f(\boldsymbol{\xi})\,\xi_1^{\nu-1}\mathrm{d}T_4 = \frac{1-v}{4\pi\,\nu}\int_{\frac{1}{1-u}}^{\frac{1}{-u}} \left\{\int_{\min}^{\max} e^{-jkR}\left(\frac{\xi_1-u}{R}\right)\mathcal{J}_\xi(\boldsymbol{\xi})\,f(\boldsymbol{\xi})\,\mathrm{d}\zeta\right\}\mathrm{d}\varphi \tag{30}$$

where, obviously, λ_E should now be computed as in Table II for the σ value given in Table III, with

$$\min = \left(u+\frac{1-\lambda_E}{\varphi}\right)^\nu \tag{31}$$

$$\max = \left(u+\frac{1}{\varphi}\right)^\nu. \tag{32}$$

Thus, although we use the polar (λ, σ) coordinates to cancel Green's function singularity, the numerical integrals are worked out in the (ζ, σ) or (ζ, φ) frame to compute, in sequence, the $\boldsymbol{\xi}$ coordinates (see Table IV) and the child coordinates of the integration point. For $0 \leq v \leq 1$, it is easily verified from Table II that the lower limit of the integral on ζ is zero for all the integrals (23)–(25), (29), and (30). The upper and lower limits of the ζ-integrals could be equal; in this case, obviously, the ζ-integrals vanish.

In passing, we observe that to integrate on T_2 and T_4 in the special case of $u = 0$, instead of using (18) and (19) in the grandparent space, it is better to work in the $\boldsymbol{\xi}$-parent space and use the transformations (see Table I)

$$\begin{aligned}&\zeta_1 = (1-\lambda)^\nu \quad \text{for } T_2 \text{ and } T_4\\ &\zeta_2 = \sigma^\nu,\ \ (1-\sigma)^\nu \quad \text{for } T_2, T_4, \text{ respectively}\end{aligned} \tag{33}$$

that yield

$$\begin{aligned}\xi_1^{\nu-1}\mathrm{d}\lambda\,\mathrm{d}\sigma &= -\frac{1}{\nu^2}\,\mathrm{d}\zeta_1\,\mathrm{d}\zeta_2 \quad \text{on } T_2\\ \xi_1^{\nu-1}\mathrm{d}\lambda\,\mathrm{d}\sigma &= +\frac{1}{\nu^2}\,\mathrm{d}\zeta_1\,\mathrm{d}\zeta_2 \quad \text{on } T_4.\end{aligned} \tag{34}$$

These transformations are not considered here since open integration routines do not sample the integrand at the integration border. However, one should keep in mind that the integrals (18) and (19) on T_2 and T_4 are likely to provide inaccurate numerical results for $u = 0$.

V. RESULTS

To test the preceding expressions, we consider a basis function of the form [18]

$$\boldsymbol{B}(\xi_1, \xi_2) = \hat{\boldsymbol{\xi}}_2\,(\xi_2-1)\left(\frac{1}{2}\xi_1^{\nu-1}-1\right) \tag{35}$$

TABLE V

NONSELF-CELL INTEGRATIONS—ADAPTIVE QUADRATURE

(x, y)	(u, v)	I	Relative Error
(0.12 , 0.12)	(1.2 , 1.2)	$4.247535998850\ 5220 \times 10^{-4} - j\,4.1155066618\ 2864 \times 10^{-5}$	9.8×10^{-14}
(0.13 , 0.05)	(1.3 , 0.5)	$9.74194559229\ 52220 \times 10^{-4} - j\,4.7333805104\ 1173 \times 10^{-5}$	1.5×10^{-13}
(-0.01 , 0.05)	(-0.1 , 0.5)	$-2.91357343917\ 91305 \times 10^{-3} + j\,2.687456941\ 35670 \times 10^{-5}$	2.1×10^{-12}
(-0.001, -0.02)	(-0.01, -0.2)	$-1.166635753675\ 3162 \times 10^{-3} + j\,2.18837064394\ 815 \times 10^{-5}$	1.2×10^{-13}
(-0.001, 0.12)	(-0.01, 1.2)	$-4.137746279325\ 8655 \times 10^{-4} + j\,2.14808542239\ 466 \times 10^{-5}$	1.9×10^{-13}
The reference I value obtained with Mathematica [24] has digits in black that agree with the adaptive quadrature of (12), and additional digits in blue. Use of nearly singular integration formulas further reduces the relative error (see Table VI).			

TABLE VI

NEARLY SINGULAR INTEGRATIONS—ADAPTIVE QUADRATURE

(x, y)	(u, v)	I	Relative Error
(0.101 , 0.05)	(1.01 , 0.5)	$2.2842151009327\ 825 \times 10^{-3} - j\,3.264790213897\ 90 \times 10^{-5}$	3.2×10^{-15}
(0.1001, 0.05)	(1.001, 0.5)	$2.42954360607\ 89998 \times 10^{-3} - j\,3.2180244697331\ 7 \times 10^{-5}$	4.3×10^{-15}
(0.05, -0.001)	(0.5, -0.01)	$1.43148045068169\ 60 \times 10^{-3} - j\,5.417642094414\ 21 \times 10^{-6}$	4.2×10^{-15}
(0.05, -0.0001)	(0.5, -0.001)	$1.58914392101678\ 78 \times 10^{-3} - j\,5.418946243847\ 34 \times 10^{-6}$	5.1×10^{-15}
The reference I value obtained with Mathematica [24] has digits in black that agree with the adaptive quadrature, and additional digits in blue.			

TABLE VII

SELF-CELL INTEGRATIONS—ADAPTIVE QUADRATURE

(x, y)	(u, v)	I	Relative Error
(0, 0)	(0, 0)	$-6.96773\ 767263747186 \times 10^{-3} + j\,2.1503682452515\ 395 \times 10^{-5}$	1.4×10^{-07}
(0, 1)	(0, 1)	$-9.217324695\ 68769916 \times 10^{-4} + j\,2.122097404086\ 5942 \times 10^{-5}$	8.7×10^{-12}
(1, 0)	(1, 0)	$2.20795487021447\ 225 \times 10^{-3} - j\,3.2022552050505\ 820 \times 10^{-5}$	1.2×10^{-15}
(1, 1)	(1, 1)	$7.4962050527395\ 1003 \times 10^{-4} - j\,3.1600676567618\ 362 \times 10^{-5}$	1.2×10^{-15}
(0.01 , 0.01)	(0.1 , 0.1)	$-5.5037306362656\ 800 \times 10^{-3} + j\,1.62064581636571 \times 10^{-5}$	1.9×10^{-15}
(0.02 , 0.02)	(0.2 , 0.2)	$-2.6006411062500\ 860 \times 10^{-3} + j\,1.083832059075\ 93 \times 10^{-5}$	1.7×10^{-15}
0.05 , 0.05)	0.5 , 0.5)	$1.79640528116042\ 01 \times 10^{-3} - j\,5.436897148887\ 63 \times 10^{-6}$	1.0×10^{-16}
(0.05 , 0.001)	(0.5 , 0.01)	$1.8032041006143\ 864 \times 10^{-3} - j\,5.42049342318\ 233 \times 10^{-6}$	1.9×10^{-15}
(0.001 , 0.001)	(0.01 , 0.01)	$-8.06202030167824\ 26 \times 10^{-3} + j\,2.097786631310\ 18 \times 10^{-5}$	2.2×10^{-16}
(0.001 , 0.05)	(0.01 , 0.5)	$-6.92424412589334\ 68 \times 10^{-3} + j\,2.104149019731\ 56 \times 10^{-5}$	1.0×10^{-15}
(0.001 , 0.099)	(0.01 , 0.99)	$-1.00062477777717\ 00 \times 10^{-3} + j\,2.0707604581502\ 5 \times 10^{-5}$	2.4×10^{-17}
The reported reference I-value are obtained with Mathematica [24] if the observer is located at one of the four cell-corners (top-part of the Table). At inner points Mathematica cannot directly integrate (12) and the reported reference results are computed by subdividing each line integrals into sixteen sub-integrals on which we use a Kronrod-Patterson integration rule starting with a formula with 127 nodes (this requires a number of samples of the order of 2,000 per line integral; that is ≈4M sampling points on each subtriangle). The reference I value has digits in black that agree with adaptive quadrature and additional digits in blue. To compute the black digits of I for an observation point on the $u = v = 0$ corner we use a (more expensive) Kronrod-Patterson rule starting with a formula with 127 nodes. (The "ad-hoc" quadrature scheme to deal with the $u = 0$ case alluded to at the end of Section IV has not been used here.)			

which exhibits a knife-edge singularity along the $\xi_1 = 0$ edge when $v = 0.5$. (This is actually a half-basis function that represents the singular behavior of the current density on one part of a two-cell pair and exhibits a normal discontinuity along edge 2 at $\xi_2 = 0$.) The testing function will be

$$\boldsymbol{T}(\xi_1, \xi_2) = \hat{\boldsymbol{\xi}}_2\, \delta(\xi_1 - u, \xi_2 - v). \tag{36}$$

The function f appearing in (6) is, therefore,

$$f(\xi_1, \xi_2) = (\xi_2 - 1)\left(\frac{1}{2} - \xi_1^{1-\nu}\right) \tag{37}$$

and Tables from V to VIII report reference results for the integral:

$$\begin{aligned} I &= \int_0^1 \int_0^1 (\xi_2 - 1)\left(\frac{1}{2\sqrt{\xi_1}} - 1\right) \frac{G(R)}{100}\, d\xi_1\, d\xi_2 \\ &= \int_0^{\frac{1}{10}} \int_0^{\frac{1}{10}} (10y - 1)\left(\frac{1}{2\sqrt{10x}} - 1\right) G(R)\, dx\, dy \end{aligned} \tag{38}$$

obtained by considering the $\nu = 1/2$ case and a source cell, 0.1 wavelength per side, located in the range $0 \le x \le 0.1$, $0 \le y \le 0.1$ of the child (x, y)-space, mapped by the parent-cell $\{0 \le \xi_1 \le 1,\ 0 \le \xi_2 \le 1\}$. The observer location (x, y) in the child space and (u, v) in the $\boldsymbol{\xi}$-parent space is given in Tables from V to VIII. The results for I reported in the Tables (V to VIII) with "black" digits are evaluated by an adaptive quadrature rule that attempts to reduce the error in the result below 10^{-11}. These are evaluated as in (12) whenever the observer location falls into the nonself-cell case, (16)–(19) are employed for the self-cell case, and (16)–(19) and (23)–(25) are used for the nearly singular case. The remaining "blue" digits of the reference result are beyond the digits obtained from adaptive quadrature using double precision. The last column of Tables V to VIII shows the error of adaptive quadrature with respect to the reference result.

The reference values are obtained by numerically integrating (12) with the Mathematica code [24] (without using the polar coordinate transformations discussed earlier) with the exception of the self-case results of Table VII that are relative

TABLE VIII

SELF-CELL INTEGRAL AT THE FOUR CORNERS

(x, y)	(u, v)	I	Relative Error
(0, 0)	(0, 0)	$-6.967737\ 67263747186 \times 10^{-3} + j\,2.1503682452515\ 395 \times 10^{-5}$	9.7×10^{-08}
(0, 1)	(0, 1)	$-9.2173246956876991\ 6 \times 10^{-4} + j\,2.12209740408659\ 42 \times 10^{-5}$	4.4×10^{-17}
(1, 0)	(1, 0)	$2.207954870214472\ 25 \times 10^{-3} - j\,3.20225520505058\ 20 \times 10^{-5}$	1.3×10^{-17}
(1, 1)	(1, 1)	$7.49620505273951\ 003 \times 10^{-4} - j\,3.1600676567618\ 362 \times 10^{-5}$	3.5×10^{-16}

This Table validates the results of Table VII. The reference I value obtained with Mathematica [24] shows digits in black that agree with results obtained by subdividing each line integral into sixteen sub-integrals on which we use a Kronrod-Patterson integration rule starting with a formula with 127 nodes, and additional digits in blue.

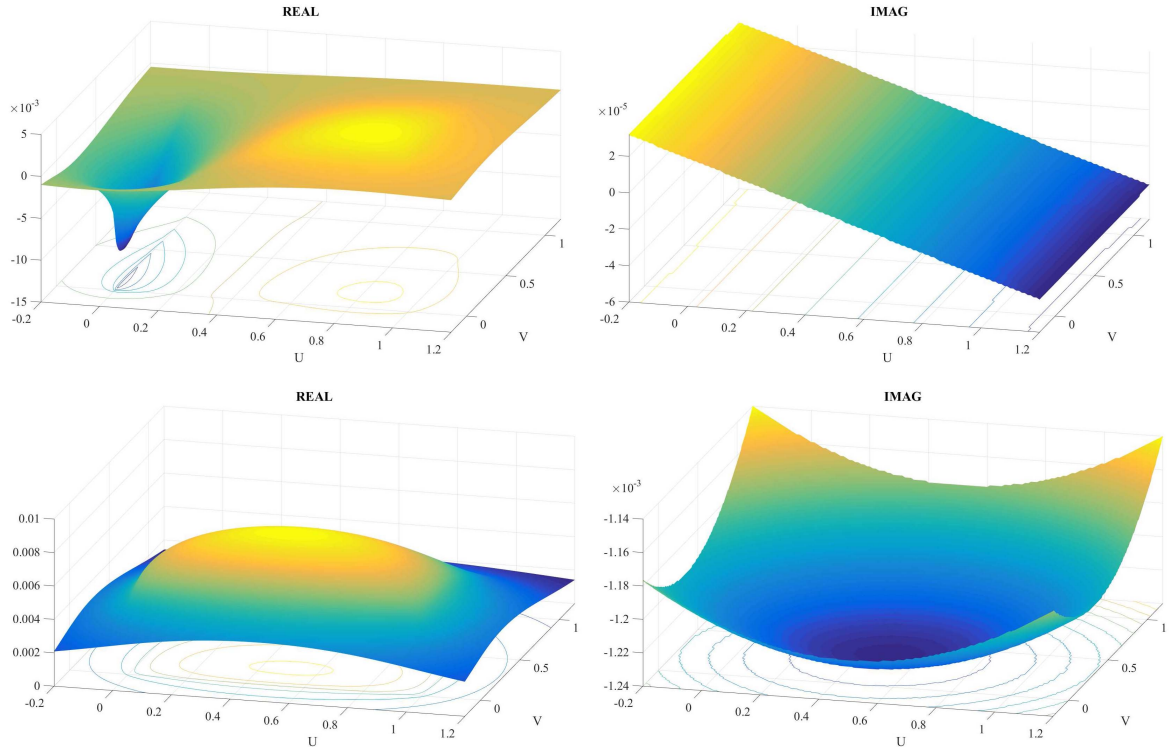

Fig. 5. Source cell, 0.1 wavelength square, is located in the range $0 \le x \le 0.1$, $0 \le y \le 0.1$ of the child (x, y)-space and is mapped by the parent cell $\{0 \le \xi_1 \le 1,\ 0 \le \xi_2 \le 1\}$. The real and imaginary parts of the integral (38) are shown at top. For the sake of comparison, the figures at bottom show the result for the nonsingular integral (39). The figures are in the $\boldsymbol{\xi}$-parent space for observation point (u, v) mapped by the child point $(x = u/10,\ y = v/10)$.

to observation points inside the cell. [Mathematica is in fact unable to numerically integrate (12) for observation points inside the cell, unless one incorporates the polar transformations given in Sections III and IV or some appropriate scheme within Mathematica.] In the self-case of Table VII, the reference values are computed by subdividing each line integral (16)–(19) into sixteen subintegrals on which we use a Kronrod–Patterson integration rule starting with a formula with 127 nodes, which requires a number of samples of the order of 2000 per line integral (about four million sampling points per subtriangle).

Table V shows results for the integral I when the observer is located outside the source cell at various positions. For these results both the nonself-cell equation (12) and the nearly singular equations were employed (even though these observers are not very near to the source cell) and gave the same result to more digits than were requested from the quadrature routines. An independent evaluation of the integral in (6) using a special quadrature rule for handling the basis function singularity also gave agreement with these results. These results indicate that the technique used in (12) for handling the basis function singularity is successful. They also indicate that the combination of (16)–(19) and (23)–(25) work well even when the observer is relatively far from the source cell.

Table VI shows various results for nearly singular integrals where the observer was slightly outside the source cell, using (16)–(19) and (23)–(25). These results are compared with the result from (12) and from an independent evaluation of the integral using a special quadrature rule for handling the basis function singularity. For these examples, attempts to evaluate (12) failed in many cases when the quadrature routine could not reduce the error below the requested tolerance (because of the proximity of the Green's function singularity). However, the evaluation of (16)–(19) and (23)–(25) was possible to a tolerance of at least 10^{-11}.

Table VII shows similar examples for self-cell integrations, where the observer lies within the source cell.

Equations (16)–(19) were employed. An independent evaluation of the integral using a different Green's function singularity cancellation scheme and a special quadrature rule for handling the basis function singularity also gave agreement with these results. These suggest that the subdivision of the cell into four triangles and the associated polar transformations are working properly to cancel Green's function singularity.

Table VIII reports the results for the case when the observer is located exactly on one of the corners of the source cell, using the "singular" equations (16)–(19). (The "*ad hoc*" quadrature scheme to deal with the $u = 0$ case was not used, because self-cell integrals are seldom evaluated on the cell border in MoM applications.) Table VIII validates the results of Table VII because the reported reference results for the corner nodes are obtained by numerically integrating (12) with the Mathematica code [24], while the black figures are computed by subdividing each line integral (16)–(19) into sixteen subintegrals on which we use a Kronrod–Patterson integration rule starting with a formula with 127 nodes, which is the same integration scheme we used to get the reference results of Table VII for observer not located on the cell corners.

Finally, Fig. 5 at top shows the real and imaginary part of the integral (38) compared with the results (reported at bottom) for the nonsingular integral

$$I = \int_0^1 \int_0^1 (\xi_2 - 1)\, G(R)\ \ d\xi_1\, d\xi_2 = \int_0^{\frac{1}{10}} \int_0^{\frac{1}{10}} (10y - 1)\, G(R)\, dx\, dy. \tag{39}$$

VI. Conclusion

New algorithms were proposed for evaluating the EFIE matrix entries in the situation, where a basis function edge singularity or the combination of an edge singularity and a Green's function singularity occur in the same quadrilateral cell. Standard singularity cancellation transformations designed for Green's function singularities are not designed to handle edge singularities. The approach is described and validated using reference results from Mathematica [24] and special quadrature rules.

References

[1] R. D. Graglia and A. F. Peterson, *Higher-Order Techniques in Computational Electromagnetics*. Edison, NJ, USA: IET, 2016.

[2] D. R. Wilton, S. M. Rao, A. W. Glisson, D. H. Schaubert, O. Al-Bundak, and C. M. Butler, "Potential integrals for uniform and linear source distributions on polygonal and polyhedral domains," *IEEE Trans. Antennas Propag.*, vol. AP-32, no. 3, pp. 276–281, Mar. 1984.

[3] R. D. Graglia, "On the numerical integration of the linear shape functions times the 3-D Green's function or its gradient on a plane triangle," *IEEE Trans. Antennas Propag.*, vol. 41, no. 10, pp. 1448–1455, Oct. 1993.

[4] L. Rossi and P. J. Cullen, "On the fully numerical evaluation of the linear-shape function times the 3D Green's function on a plane triangle," *IEEE Trans. Microw. Theory Techn.*, vol. 47, no. 4, pp. 398–402, Apr. 1999.

[5] A. Herschlein, J. V. Hagen, and W. Wiesbeck, "Methods for the evaluation of regular, weakly singular and strongly singular surface reaction integrals arising in method of moments," *Appl. Comput. Electromagn. Soc. J.*, vol. 17, no. 1, pp. 63–73, Mar. 2002.

[6] D. J. Taylor, "Accurate and efficient numerical integration of weakly singular integrals in Galerkin EFIE solutions," *IEEE Trans. Antennas Propag.*, vol. 51, no. 7, pp. 1630–1637, Jul. 2003.

[7] M. A. Khayat and D. R. Wilton, "Numerical evaluation of singular and near-singular potential integrals," *IEEE Trans. Antennas Propagat.*, vol. 53, no. 10, pp. 3180–3190, Oct. 2005.

[8] R. D. Graglia and G. Lombardi, "Machine precision evaluation of singular and nearly singular potential integrals by use of gauss quadrature formulas for rational functions," *IEEE Trans. Antennas Propag.*, vol. 56, no. 4, pp. 981–998, Apr. 2008.

[9] G. Lombardi, "Design of quadrature rules for Müntz and Müntz-logarithmic polynomials using monomial transformation," *Int. J. Numer. Methods Eng.*, vol. 80, no. 13, pp. 1687–1717, 2009.

[10] M. S. Tong and W. C. Chew, "A novel approach for evaluating hypersingular and strongly singular surface integrals in electromagnetics," *IEEE Trans. Antennas Propag.*, vol. 58, no. 11, pp. 3593–3601, Nov. 2010.

[11] A. G. Polimeridis and J. R. Mosig, "Evaluation of weakly singular integrals via generalized Cartesian product rules based on the double exponential formula," *IEEE Trans. Antennas Propag.*, vol. 58, no. 6, pp. 1980–1988, Jun. 2010.

[12] A. G. Polimeridis and J. R. Mosig, "Complete semi-analytical treatment of weakly singular integrals on planar triangles via the direct evaluation method," *Int. J. Numer. Methods Eng.*, vol. 83, no. 12, pp. 1625–1650, Sep. 2010.

[13] S. A. Sauter and C. Schwab, *Boundary Element Methods*. Berlin, Germany: Springer-Verlag, 2011, ch. 5, doi: 10.1007/978-3-540-68093-2.

[14] M. Lenoir and N. Salles, "Evaluation of 3-D singular and nearly singular integrals in Galerkin BEM for thin layers," *SIAM J. Sci. Comput.*, vol. 34, no. 6, pp. A3057–A3078, 2012.

[15] F. Vipiana, D. R. Wilton, and W. A. Johnson, "Advanced numerical schemes for the accurate evaluation of 4-D reaction integrals in the method of moments," *IEEE Trans. Antennas Propag.*, vol. 61, no. 11, pp. 5559–5566, Nov. 2013.

[16] D. R. Wilton, F. Vipiana, and W. A. Johnson, "Evaluation of 4-D reaction integrals in the method of moments: Coplanar element case," *IEEE Trans. Antennas Propag.*, vol. 65, no. 5, pp. 2479–2493, May 2017.

[17] D. Tihon and C. Craeye, "All-analytical evaluation of the singular integrals involved in the method of moments," *IEEE Trans. Antennas Propag.*, vol. 66, no. 4, pp. 1925–1936, Apr. 2018.

[18] R. D. Graglia and G. Lombardi, "Singular higher order divergence-conforming bases of additive kind and moments method applications to 3D sharp-wedge structures," *IEEE Trans. Antennas Propag.*, vol. 56, no. 12, pp. 3768–3788, Dec. 2008.

[19] R. D. Graglia, G. Lombardi, D. R. Wilton, and W. A. Johnson, "Modeling edge singularities in the method of moments," in *Proc. IEEE AP-S Int. Symp.*, vol. 3A, Jul. 2005, pp. 56–59.

[20] R. D. Graglia, A. F. Peterson, and P. Petrini, "Hierarchical singular vector bases for quadrilateral cell MoM applications," in *Proc. Int. Conf. Electromagn. Adv. Appl. (ICEAA)*, Verona, Italy, Sep. 2017, pp. 1929–1932.

[21] M. G. Duffy, "Quadrature over a pyramid or cube of integrands with a singularity at a vertex," *SIAM J. Numer. Anal.*, vol. 19, no. 6, pp. 1260–1262, 1982.

[22] M. Stern and E. B. Becker, "A conforming crack tip element with quadratic variation in the singular fields," *Int. J. Numer. Methods Eng.*, vol. 12, no. 2, pp. 279–288, 2008.

[23] R. D. Graglia, A. F. Peterson, and P. Petrini, "Hierarchical divergence conforming bases for edge singularities in quadrilateral cells," *IEEE Trans. Antennas Propag.*, vol. 67, no. 11, pp. 6191–6201, Nov. 2018.

[24] *Mathematica, Version 8.0*, Wolfram Research, Inc., Champaign, IL, USA, 2010.

Roberto D. Graglia, photograph and biography not available at the time of publication.

Andrew F. Peterson, photograph and biography not available at the time of publication.

Paolo Petrini, photograph and biography not available at the time of publication.